INTERNATIONAL RESEARCH JOURNAL OF AUTOMOTIVE TECHNOLOGY (IRJAT)

http://www.mapletreejournals.com/index.php/IRJAT
Received 22 November 2018 ISSN 2581-5865
Accepted 29 November 2018 2018; 1(6);60-79
Published online 30 November 2018

# Numerical Simulation of Mixing and Combustion of a Hydrogen Fueled Scramjet combustor using Strut Injectors

**M. Manoj Kumar[1*], Dr. T. Siva Sakthi [2], K. Deniyal [3]**

[1] *Assistant Professor, Department of Mechanical Engineering, Amrita College of engineering and technology Nagercoil, Kanyakumari District.*

[2] *PDF Scholar, Department of Chemical Engineering, Wuhan University of technology, China[2]*

[3]UG Scholar, *Department of Mechanical Engineering, Amrita College of engineering and technology, Nagercoil, Kanyakumari, District*

**Corresponding author E-Mail ID: manoj0728@gmail.com, Mobile: 9894434864*

## ABSTRACT

A major problem in supersonic combustion is the short residence time of the fluid inside the combustor due to high flow velocities. Thus techniques for mixing enhancement have to be used to achieve a fast and efficient fuel-air mixing. In the present project work, different types of strut fuel injectors are investigated numerically, mainly strut with circular injector, strut with planer injector and strut with alternating wedge injector. The combustor and strut dimensions are same as DLR Scramjet model. It consists of a divergent channel with a flame – holding, wedge shaped structure in the middle of the flow field from the base of which hydrogen is injected. Study of mixing and combustion enhancement has been performed for a Mach 2 and Fuel (hydrogen) is injected at supersonic speed of Mach 1. The simulations have been performed using FLUENT. Standard k-ε model has been used for modeling turbulence and single step finite rate chemistry has been used for modeling the H2-Air kinetics. k- ε model is based on a finite volume discretization of the continuity, momentum, energy equations. Numerically predicted profiles of static pressure, axial velocity, turbulent kinetic energy and static temperature for both non-reacting as well as reacting flows are compared with each other models. For the purpose of validation, the k-ε results are compared with experimental data. In addition, qualitative comparisons are also made between predicted and measured shadowgraph images. It was found that mixing and combustion with a less flow-disturbing strut was considerably worse than those with a more flow-disturbing strut. Additionally, changes are caused within the shock-wave/expansion wave pattern at the injector exit that has an important influence on loss in total pressure.

## 1. INTRODUCTION

The name scramjet is an acronym for Supersonic Combustion Ramjet. A scramjet engine, is a type of jet engine intended to operate in the high velocity regime usually associated with rockets. The Scramjet engine design is an extension of the Ramjet. The difference between the two lies in flow state inside the engine. Both are designed to be used for supersonic flight; however a Scramjet allows the flow through the engine to remain supersonic, whereas in a Ramjet

the flow is slowed to subsonic levels before it enters the combustor. Fig.1 shows a basic generic Scramjet design. It works by injecting fuel (typically hydrogen) into a flow of supersonic air. The air is at sufficiently high temperature and pressure for the fuel to combust, and the resulting mixture is expelled from the engine at a higher pressure. The Scramjet is composed of four main sections: the inlet, isolator, combustor and exhaust nozzle. These sections can be seen in Fig.1

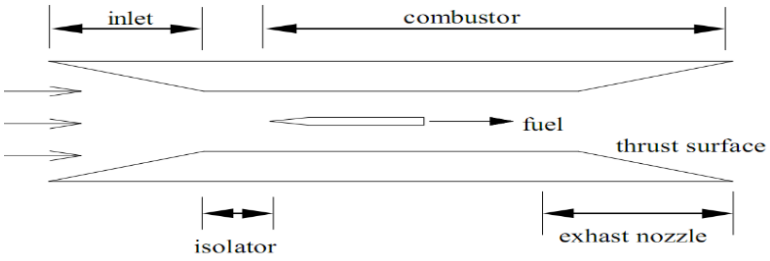


***Fig.1. Generic Scramjet engine***

The inlet heats and slows the flow through a series of oblique shockwaves. This "ram" portion of the cycle means the engine cannot be operated statically. The isolator serves to separate the combustor from the inlet of the engine, allowing further slowing of the flow. Combustion is achieved through the continuous injection of fuel (usually hydrogen) into the supersonic flow. The fuel mixes and combusts, increasing the pressure and temperature of the flow. Finally the flow is expanded via the nozzle. This serves two purposes: to allow the flow to accelerate to the external speed, and to provide a mechanism by which the increase in pressure can be converted into forward thrust.

## 2. THEORY

This chapter gives a short description of the theory behind supersonic flow and Computational Fluid Dynamics.

### 2.1 Supersonic Flow Theory

The most important consideration with supersonic flow is that the flow is compressible. A compressible flow is one for which the density cannot be considered constant (for flow below M = 0.3 the fluid can be considered to have a constant density). Compressibility leads to two phenomena unique to supersonic flow - shockwaves and expansion waves Fig.2. There are two types of shockwaves: oblique and normal. Oblique shockwaves and expansion waves are generated when a supersonic flow changes direction – a shockwave when the flow converges and an expansion wave when the flow expands.

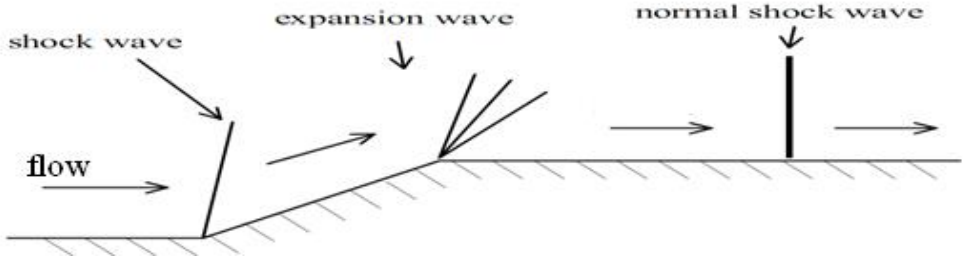


***Fig.2 Shock and Expansion Waves***

## 3. OBLIQUE SHOCK WAVE

An oblique shockwave is generated when the direction of a supersonic flow changes in a convergent way. The relative conditions after an oblique shock are the same as for the normal shock – Mach number decreases and pressure, temperature, density and entropy increase. The flow can however remain supersonic. The simplest case is flow over a half wedge.

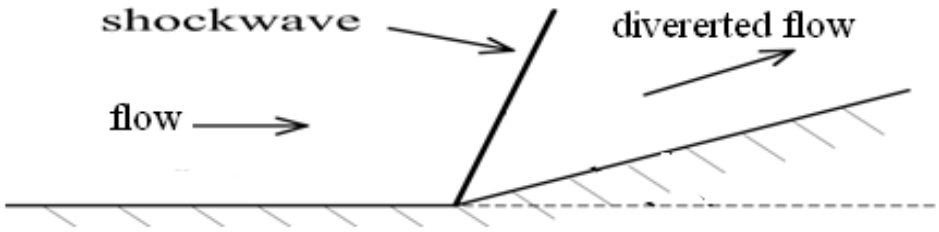


***Fig.3 Oblique shockwave***

## 4. EXPANSION WAVE

The overall effect of an expansion wave is the opposite of a shockwave: Mach number increases and temperature, pressure and density decrease. Entropy however remains constant. Unlike a shockwave, the flow condition across an expansion wave change gradually.

## 5. EQUIVALENCE RATIO

When referring to the Scramjet engine the term ‘equivalence ratio’ is often used. The equivalence ratio is a measure of the ‘richness’ of the air-fuel mixture. It is defined as the mass flux of fuel divided by the mass flux of air, all divided by this same ratio for a stoichiometric mixture.

## 6. COMPUTATIONAL FLUID DYNAMICS

CFD is a computational software tool for analysis and calculation of fluid mechanical processes, such as mass, heat and momentum transfer. The numerical method most frequently used is the finite volume method. This method is used by both software tools utilized in this thesis work.

## 7. GOVERNING EQUATIONS OF CFD

Each CFD software package has to produce a prediction of the way in which a fluid will flow for a given situation. To do this the package must calculate numerical solutions to the equations that govern the flow of fluids. For the analyst, therefore, it is important to have an understanding of both the basic flow features that can occur, and so must be modeled, and the equations that govern fluid flow. The physical aspects of any fluid flow and heat transfer are governed by three fundamental principles.

- Continuity equation, Momentum equation and Energy equation.

### 7.1 Continuity Equation

The continuity equation is essentially the equation for the conservation of mass. It is derived by the mass balance on the fluid entering and leaving a volume element taken in the flow field. The equation for the conservation of mass for two dimensional steady flows may be stated as

$$\begin{bmatrix}\text{Net rate of mass flow entering}\\ \text{volume element in x direction}\end{bmatrix} + \begin{bmatrix}\text{Net rate of mass flow entering}\\ \text{volume element in y direction}\end{bmatrix} = 0 \qquad (3.1)$$

For an incompressible fluid, the continuity equation for a steady two dimensional flow can be written as

$$\frac{\partial U}{\partial X} + \frac{\partial V}{\partial Y} = 0 \qquad (3.2)$$

### 7.2 Momentum Equation

The momentum equation are derived from Newton's second law of motion, which states that mass times the acceleration in a given direction is equal to the external force acting on the body in the same direction. The external force acting on the volume element in a flow field is considered to consist of the body forces and the surface forces.

$$[\text{Mass}]\begin{bmatrix}\text{Acceleration in}\\ \text{i direction}\end{bmatrix} = \begin{bmatrix}\text{Body forces acting in}\\ \text{i direction}\end{bmatrix} + \begin{bmatrix}\text{Surface force acting}\\ \text{in i direction}\end{bmatrix} \qquad (3.3)$$

X Momentum: $\rho\left[u\frac{\partial u}{\partial x} + v\frac{\partial u}{\partial y}\right] = F_x - \frac{\partial p}{\partial x} + \mu\left[\frac{\partial^2 u}{\partial x^2} + \frac{\partial^2 u}{\partial y^2}\right]$

Y Momentum: $\rho\left[u\frac{\partial v}{\partial x} + v\frac{\partial v}{\partial y}\right] = F_y - \frac{\partial p}{\partial y} + \mu\left[\frac{\partial^2 v}{\partial x^2} + \frac{\partial^2 v}{\partial y^2}\right]$

Where Fx and Fy are the body forces per unit volume acting in the x and y direction respectively.

The physical significance of the various terms in equation (3.4) is as follows: The terms on the left hand side represent the inertia forces, the first term on the right hand side is the body forces, the second term is the pressure forces, and the last term in the parentheses is the viscous force on the fluid element.

### 7.3 ENERGY EQUATION

The temperature distribution in the flow field is governed by the energy equation, which can be derived by writing an energy balance according to first law of thermodynamics for a differential volume element in the flow field. If radiation is absent and there are no distributed energy sources in the fluid, the energy balance on a differential volume element may be stated as

$$\begin{bmatrix}\text{rate of energy}\\ \text{input due to}\\ \text{conduction}\end{bmatrix}+\begin{bmatrix}\text{rate of energy}\\ \text{input due to}\\ \text{work done by}\\ \text{conduction}\end{bmatrix}+\begin{bmatrix}\text{rate of energy}\\ \text{input due to}\\ \text{work done by}\\ \text{surface stress}\end{bmatrix}=\begin{bmatrix}\text{rate of increase}\\ \text{of energy in}\\ \text{element}\end{bmatrix} \quad (3.6)$$

The energy equation for two dimensional flow of an incompressible, constant property, Newtonian fluid is determined as

$$\rho c_p\left[u\frac{\partial T}{\partial x}+v\frac{\partial T}{\partial y}\right]=k\left[\frac{\partial^2 T}{\partial x^2}+\frac{\partial^2 T}{\partial y^2}\right]+\mu\phi$$

Where the viscosity-energy-dissipation function $\phi$ is defined as

$$\phi=2\left[\left(\frac{\partial u}{\partial x}\right)^2+\left(\frac{\partial v}{\partial y}\right)^2\right]+\left(\frac{\partial u}{\partial x}+\frac{\partial v}{\partial y}\right)^2$$

## 8. METHODS OF DISCRETIZATION

There are several methods of discretizing a given differential equation. Some of the discretization methods being used are Finite Volume Method (FVM): This is the "classical" or standard approach used most often in commercial software and research codes. The governing equations are solved on discrete control volumes. FVM recasts the PDE's (Partial Differential Equations) of the N-S equation in the conservative form and then discretize this equation. This guarantees the conservation of fluxes through a particular control volume. Though the overall solution will be conservative in nature there is no guarantee that it is the actual solution. Moreover, this method is sensitive to distorted elements which can prevent convergence if such elements are in critical flow regions. This integration approach yields a method that is inherently conservative (i.e. quantities such as density remain physically meaningful).

$$\frac{\partial}{\partial t}\iiint Q\,dV+\iint F\,dA=0$$

Where $Q$ is the vector of conserved variables, $F$ is the vector of fluxes, $V$ is the cell volume, and $A$ is the cell surface area.

Finite element method (FEM): This method is popular for structural analysis of solids, but is also applicable to fluids. The FEM formulation requires, however, special care to ensure a conservative solution. The FEM formulation has been adapted for use with the Navier-Stokes equations. Although in FEM conservation has to be taken care of, it is much more stable than the FVM approach. Subsequently it is the new direction in which CFD is moving. Generally, stability/robustness of the solution is better in FEM though for some cases it might take more memory than FVM methods.

In this method, a weighted residual equation is formed:

$$R_i=\iiint W_i Q\,dV^e$$

Where $R_i$ is the equation residual at an element vertex i, Q is the conservation equation expressed on an element basis, $W_i$ is the weight factor and $V^e$ is the volume of the element.

Finite difference method: This method has historical importance and is simple to program. It is currently only used in few specialized codes. Modern finite difference codes make use of an embedded boundary for handling complex geometries making these codes highly efficient and accurate. Other ways to handle geometries are using overlapping-grids, where the solution is interpolated across each grid.

$$\frac{\partial Q}{\partial t}+\frac{\partial F}{\partial x}+\frac{\partial G}{\partial y}+\frac{\partial H}{\partial z}=0$$

Where $Q$ the vector of is conserved variables, and $F, G, H$ are the fluxes in the x, y, and z directions respectively.

## 9. TURBULENCE MODELING

Turbulence occurs when the inertial forces in a fluid becomes considerable relative to the viscous forces, and is characterized by a high Reynolds number. The most common turbulence modeling approach and also the one used in this thesis is the Reynolds-averaged Navier-Stokes models. RANS is based on a statistical treatment of the flow. More precise, this means that some of the variables that govern the flow are divided into a time-averaged component of the flow and a fluctuating component that represents the deviation from the mean flow. A very successful and widely employed turbulence model is k-ε model. It is a two-equation model meaning that it includes two extra transport equations to represent the turbulent properties of the flow.

Combustion modeling, the most common combustion modeling approach and also the one used in this thesis is the eddy dissipation model. It is based on the assumption that chemical reactions are fast relative to the transport processes of the flow. When the reactants mix at a molecular level they instantaneously form products. The model assumes that the reaction rate may be directly related to the time required to mix the reactants at the molecular level.

## 10. REACTION MECHANISMS

In this thesis single step reaction model (instantaneous model) were used. The fundamental concepts behind these are outlined below. The instantaneous reaction model assumes that a single chemical reaction occurs and proceeds instantaneously to completion. The reaction used for the Scramjet was the hydrogen-water reaction:

$$2H2 + O2 \rightarrow 2H2O$$

## 11. METHODOLOGY AND SOLUTION PROCEDURE

### 11.1 The DLR Scramjet Experimental Rig

A schematic of the scramjet experimental facility is presented in Fig.4.1. Preheated air is expanded through a Laval nozzle, and enters the combustor section at Ma=2.0. The combustor has a width of 40 mm and a height of 50 mm at the entrance and a divergence angle of the upper channel wall of three degrees to compensate for the expansion of the boundary layer. A wedge shaped strut is placed in the center of the combustion chamber downstream of the nozzle. The height of the 32 mm long strut is 6 mm. along the first 100 mm downstream of the Laval nozzle; the side walls and the upper wall are made from quartz glass to allow optical access and to minimize the reflection of scattered light on the wall opposite the observation window. Hydrogen (H2) is injected at Ma=1.0 through a row of 15 holes in the strut base, having a diameter of D=1.0 mm and a distance between adjacent holes of 2.4 mm. Typical mass flows in the experiments were varied between 1.0 kg/s and 1.5 kg/s for the air and between 1.5 g/s and 4.0 g/s for hydrogen. In the present work we focus on a case with a hydrogen jet velocity of vJ=1200 m/s and an airstream velocity of vA=730 m/s, corresponding to mass flows of about 1.0 g/s for the hydrogen jet and 1.0 kg/s for the air, given the densities ρH2=0.097 kg/m3 and ρair =1.002 kg/m3. The hydrogen is injected at ambient temperature and pressure, i.e. at TJ=250 K and pJ=105 Pa, whereas the air was injected at TA=340 K at pA=105 Pa, respectively. Combustion was initiated by pre-burning of a small amount of O2 in an H2 tube by a spark, which was turned off after ignition.


*Fig.4. Schematic overview of the dlr scramjet rig.*

### 11.2 Computational Configuration

The geometry considered in this project work is the same as the one considered by Oevermann [44]. The computational configuration is simplified in the sense of, all the gambit modelings are done in 3D and fluent analyses are done in 2D. The reason for this simplification is that to reduce the computational time as much as possible, but still retaining all relevant physics of the scramjet combustor.

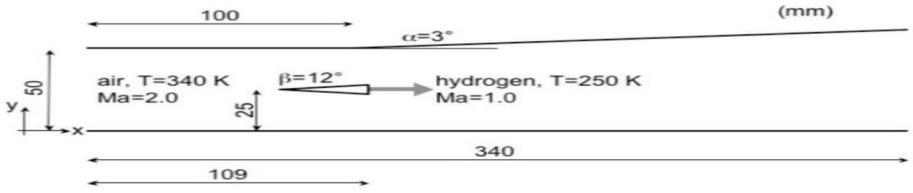


*Fig.5 Schematic overview of the supersonic combustion chamber [44]*

### 11.2.1 Computational Configuration of Strut with Circular Injector

A strut with circular injector is placed in the combustion chamber downstream of the nozzle. The height of the 32 mm long strut is 6 mm and diameter of the injector is 2.23mm.

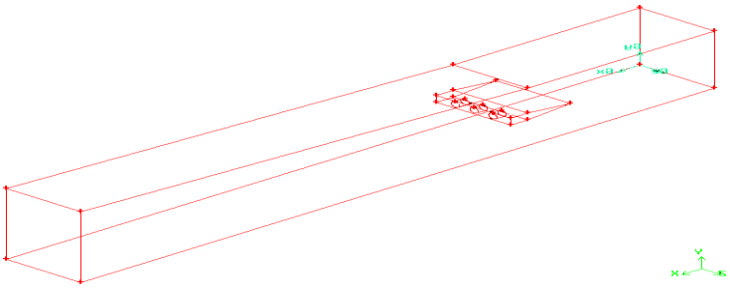

*Fig.6 Scramjet combustion chamber and strut with circular injector*

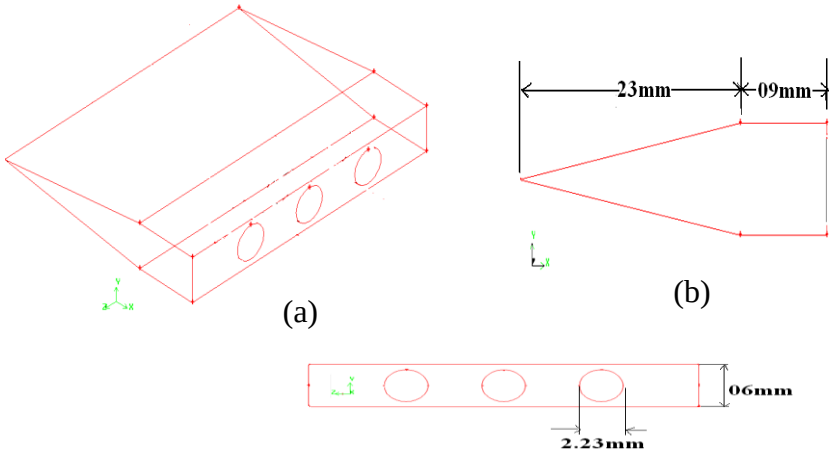


*Fig.7 Strut with circular injector*

### 11.2.2 Computational Configuration of Strut with Planer Injector

A strut with planer injector is placed in the combustion chamber downstream of the nozzle. The length of the strut is 32 mm and diameter of the injector is 0.295 mm.

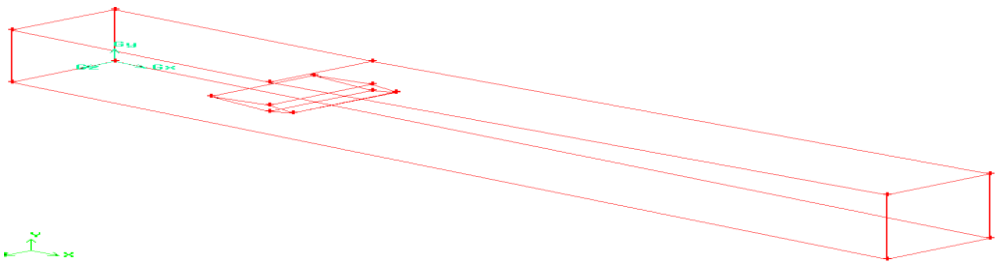

**Fig.8 Scramjet combustion chamber and strut with planer injector**

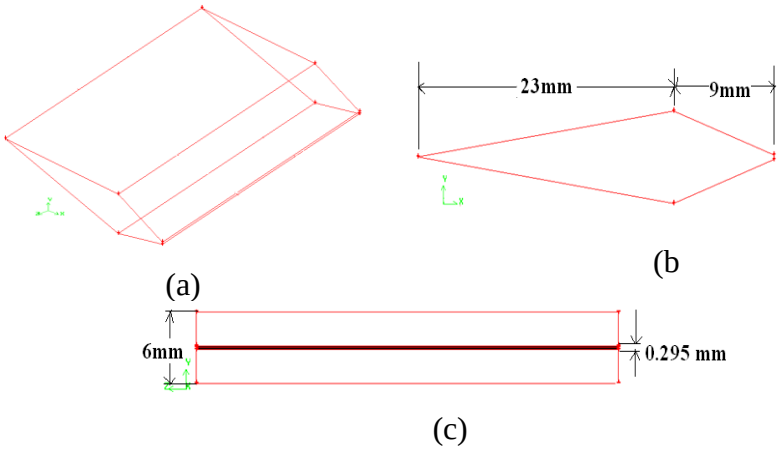


*Fig.9 Strut with planer Injector*

### 11.2.3 Computational Configuration of Strut with Alternating Wedge Injector

A strut with alternating wedge injector is placed in the combustion chamber downstream of the nozzle. The length of the strut is 32 mm and diameter of the injector is 0.295 mm.

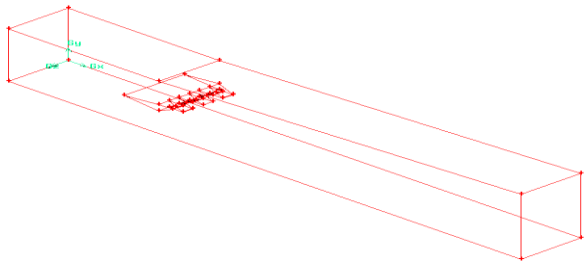

*Fig.10 Scramjet combustion chamber and strut with alternating wedge injector*

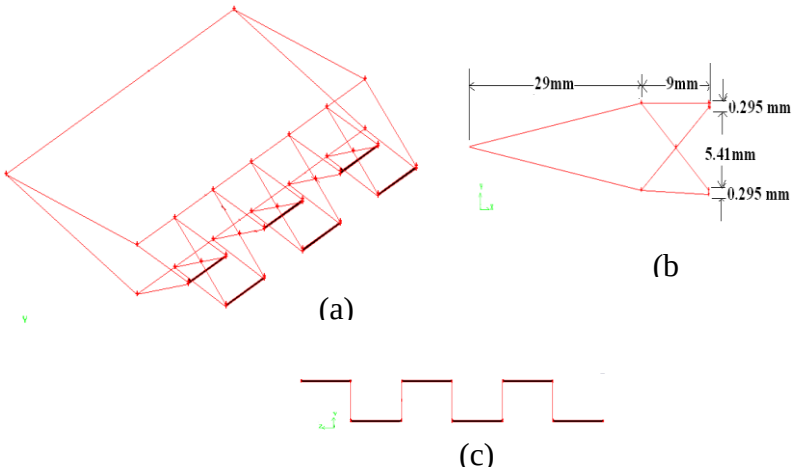


*Fig.11 Strut with alternating wedge injector*

### 11.3 Boundary Conditions

In the present study three different types of boundaries are applied: inflow, outflow and fixed walls. The flow fields under consideration here are supersonic. According to the theory of characteristics all variables are prescribed at inflow boundaries, i.e. Dirichlet boundary conditions, and Neumann boundary conditions are used for all variables at outflow boundaries. At fixed walls the no slip condition are applied. All computations are initialized with the state of the incoming air.

***Table 1 Inflow conditions of the air stream and hydrogen jet.***

| S.No | Variables | Air | Hydrogen |
|---|---|---|---|
| 1 | Ma | 2.0 | 1.0 |
| 2 | U [ m/s] | 730 | 1,200 |
| 3 | T [k] | 340 | 250 |
| 4 | P [ 105 Pa] | 1.0 | 1.0 |
| 5 | ρ [ kg/m3] | 1.002 | 0.097 |
| 6 | Yo2 | 0.232 | 0 |
| 7 | YN2 | 0.736 | 0 |
| 8 | YH2o | 0.032 | 0 |
| 9 | YH2 | 0 | 1.0 |
| 10 | k [m2/s2] | 10 | 2400 |
| 11 | ε [m2/s3] | 650 | 108 |
| 12 | Mass flow Rate[kg/s] | 1.5 | 0.0015 to 0.004 |

### 11.4 Mesh Generation

Numerical calculations of the flow with fuel injection but without chemical reaction were first carried out on a base grid with 205,460 tetrahedral cells. This grid was then refined by adaption based on gradients of static pressure to capture the shocks, followed by refinement near all the no-slip surfaces to resolve the boundary layers well. The grid was further refined in the shear layer between the hydrogen jet and the incoming air so as to resolve the mixing and diffusion effects of hydrogen effectively. This refinement resulted in grids with 281,431 cells. For reacting flow calculations the grid was adapted further based on the gradients of reacting species so as to resolve the combustion phenomenon in the flow field accurately. After refinement, a grid with 340,840 cells has been taken as the final grid for all subsequent calculations.

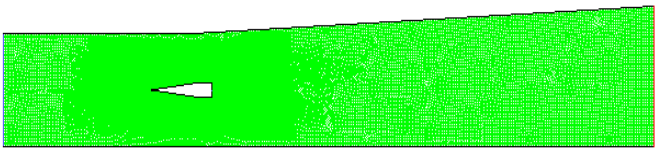

*Fig.12 Mesh generation in 2D combustion chamber*

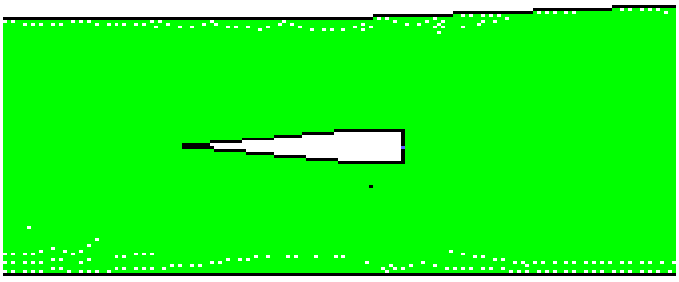

*Fig.11 Mesh generation around the strut injector*

### 11.5 Grid Independence Test

The grid independence test is carried out for analyzing the effect of grid number on the bottom wall static pressure with combustion chamber length. As illustrated in Fig.4.11, a good agreement is observed between 4, 00,000 cells and 3, 40,840 cells. Hence, the present analysis is carried out using a minimum grid size of 3, 40,840 cells.

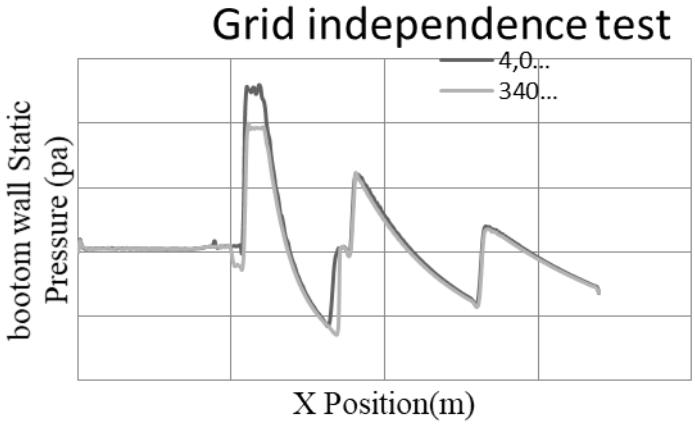


*Fig.12 Grid independence test*

### 11.6 NUMERICAL SOLUTION

The inlet conditions of the H2 injection ports are adjusted so as to achieve sonic injection with the desired fuel mass flow rate. The equivalence ratio is 0·0125. The flow through the combustor is compressible and three-dimensional. In addition, turbulence and finite rate chemistry are also considered. k-ε model is used for modeling turbulence with default values for the

constants (C1ε = 1·44, C2ε = 1·9). The turbulent Prandtl and Schmidt numbers have been assumed to be 1·2, 0·7 respectively. Single step, finite rate kinetics has been used to model chemistry. Viscosity and Cp of the mixture have been evaluated using mass-weighted mixing law. Adiabatic boundary conditions with standard wall functions have been used on all the wall surfaces. Stagnation temperature and pressure for the vitiated air are 612K and 7·825 bar respectively. In addition, k and ε have been specified [44].

## 12. RESULTS AND DISCUSSIONS

The results from the numerical simulations for strut with circular injector, strut with planer injector and strut with alternating wedge injector are described under three categories namely (i) non reacting flow (hydrogen injection but without combustion), (ii) reacting flow (hydrogen injection with combustion), and (iii) performance measures. All the simulations are started with incoming air.

### 12.1 Performance measures

In this section, for assessing the overall performance of the combustor, namely, mixing efficiency and combustion efficiency are discussed.

### 12.2 Mixing efficiency

Fuel is injected from the base of the wedge at x ≈ 0·111m and the mixing is complete at x ≈ 0·160m. The contours of mass fraction of H2 are shown in Fig.5.29 and Fig.5.30. It also indicates that mixing taking place rapidly.

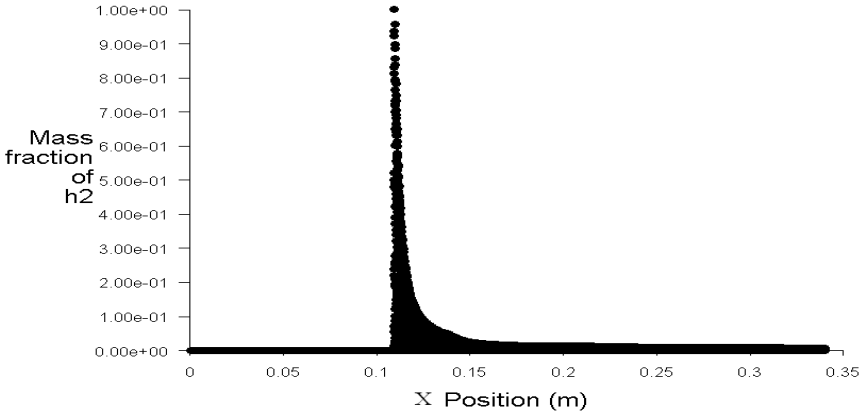


***Fig.13 Mass Fraction of $H_2$***

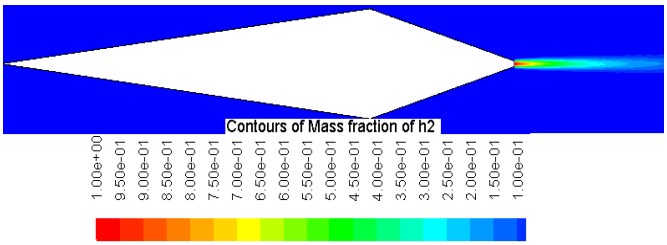


***Fig.14 Contours of $H_2$***

Comparing the mixing efficiency of the planer injector with circular injector we can observe that there are some changes in the flow field. In circular injector the mixing are over at x=225mm but in planer injector the mixing is over at x =160mm. from this it is clear that strut with planer injector giving good mixing efficiency.

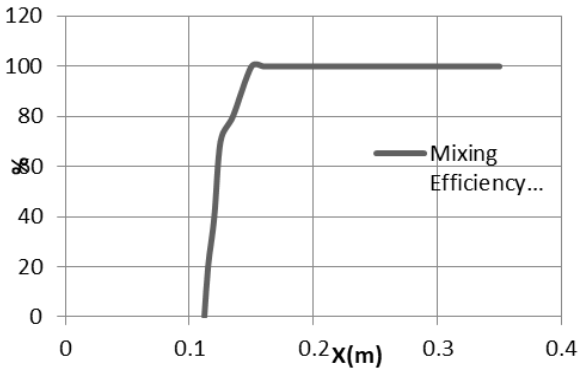


***Fig.15 Mixing Efficiency***

## 13. COMBUSTION EFFICIENCY

It appears from Fig.5.34 that combustion is complete at x ≈ 0·170m. Contours of the mass fraction of H2O are given in Fig.5.32 and Fig.5.33. It can be seen that the maximum value for the mass fraction of H2O is reached at a distance of 0·165m, which is just downstream of the wedge. However, the distribution of the mass fraction of H2O continues to change till 0·290m, beyond which it remains the same.

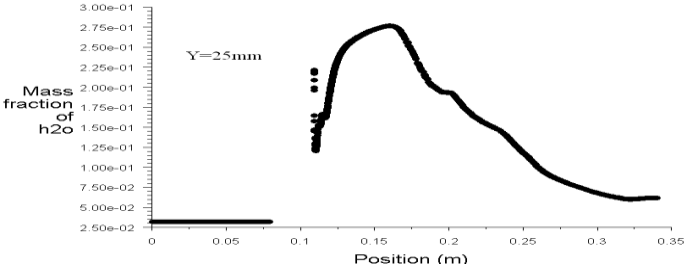


***Fig.16 Mass fraction of H2O***

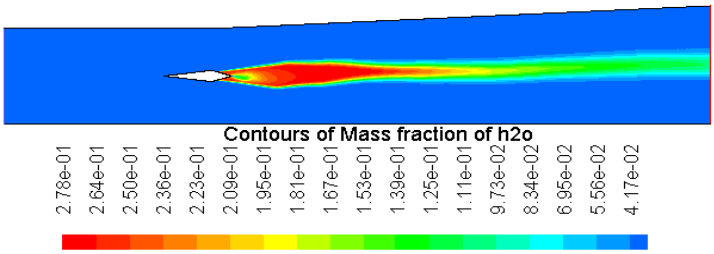


***Fig.17 Contours of H2O***

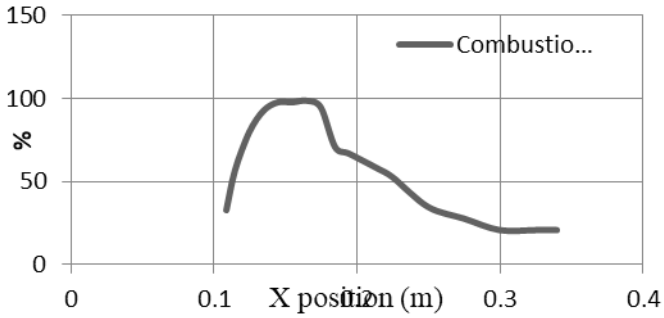


***Fig.18 Combustion efficiency***

## 14. STRUT WITH ALTERNATING WEDGE INJECTOR

### 14.1 Non-reacting (mixing) flow

Fig.19 shows the pressure contours for the non-reacting simulation. The shock generated from the blunt nose of strut and its multiple reflections from the wall boundaries can be seen clearly. As compare to other two models the effect of oblique shock wave in this model is less but the effect of expansion wave is more in this method of injection.

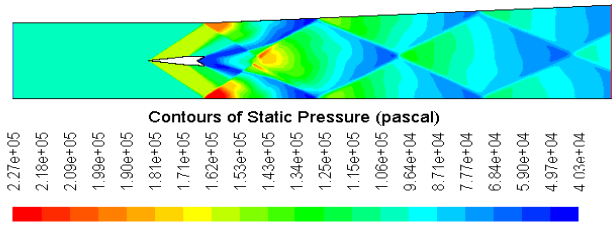


***Fig.19 Contours of static pressure***

Fig.20 shows the pressure variation at the bottom and top of the combustion chamber, it is clear that bottom wall pressure is high as compare to top wall temperature. In all the three injection method there are three pressure rise in top and bottom wall of the combustor because of shock and expansion waves.

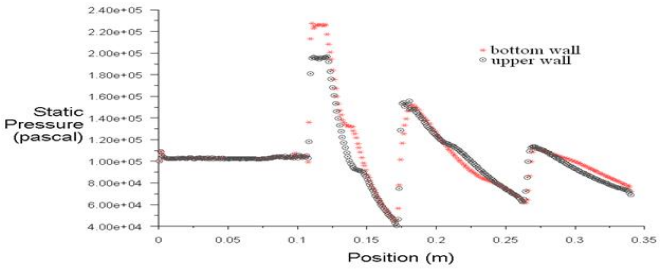


***Fig.20 Pressure Variation at the Bottom and Top Walls***

From the Mach contour shown in Fig.21 the boundary layer can be seen clearly. Also there is Mach number increases in the divergent portion of the combustor due to expansion. Also small subsonic zone can be seen in the figure which acts as a flame holding device for reacting case. As compare with the entire models, the sub sonic region in this model very small.

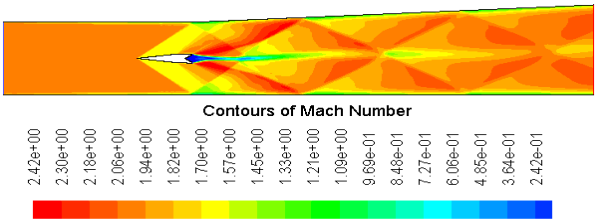


***Fig.21 Mach contour***

Fig.22 show the velocity variation at x= 120mm and x=170mm because of the shock waves interaction at x=120mm the velocity is below inlet velocity but at X=170mm the velocity variation is very less.

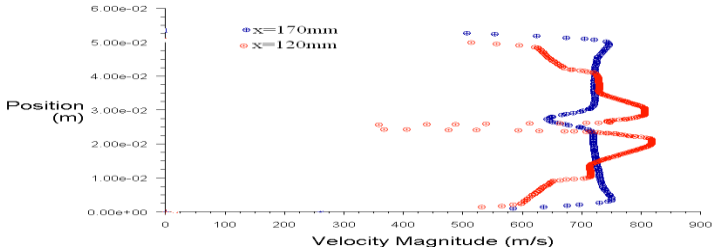


***Fig.22 velocity variation at x=120mm and x=170mm***

Fig.23 show the total pressure contours of the combustor. It can be seen that because of strut there is considerable losses in the core region of the combustor.

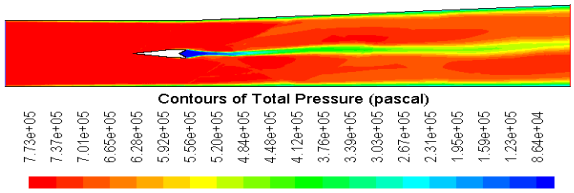


***Fig.23 Total pressure contours***

## 14.2 REACTING FLOW

Fig 24 show the pressure contours for the reacting case. The shock due to injection of fuel and its reflection from the wall boundary can be seen clearly.

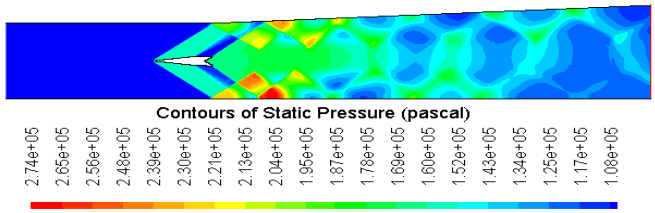


***Fig.24 Reacting flow pressure contours***

Fig.25 show the pressure variation at y= 10mm, y=25mm and y=40mm among this three the effect of oblique shock wave is higher at y=10mm.at the centre of the combustor variation of static pressure is not much high.

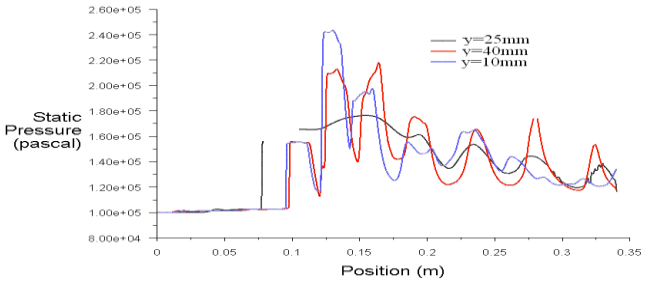


***Fig.25 Pressure variation at y= 10mm, y=25mm and y=40mm***

The Mach contours are shown in Fig.26 Comparing the reacting flow with the non-reacting case there is an increase in the low subsonic zone it will allow to mix fuel and air completely.

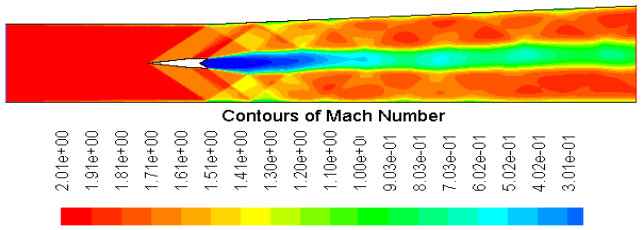


***Fig.26 Reacting flow Mach contours***

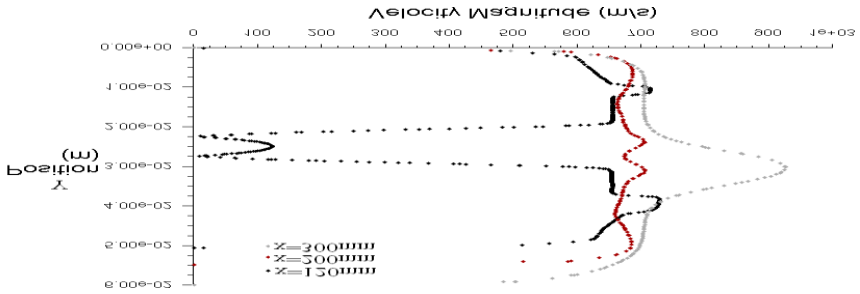


*Fig.27 Reacting flow velocity variation at x=120mm, x=200mm and x=300mm*

Fig.28 show the contours of static temperature where a small high temperature zone near the strut can be seen clearly.

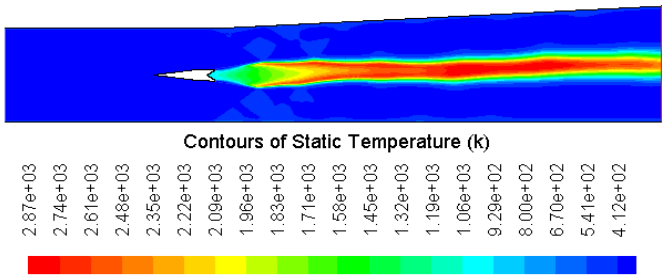


*Fig.28 Reacting flow static temperature*

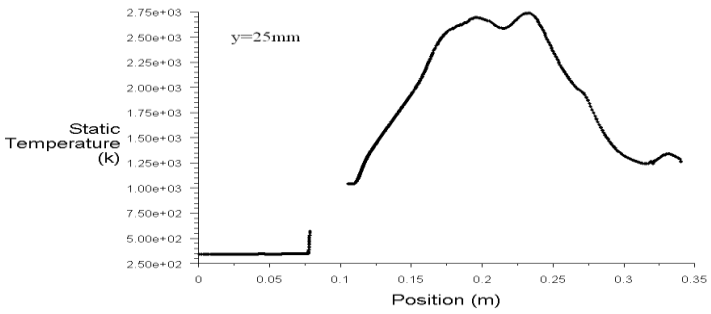


*Fig.29 Static temperature variation at y=25mm*

## 14.3 Performance Measures

In this section, for assessing the overall performance of the combustor, namely, mixing efficiency and combustion efficiency are discussed.

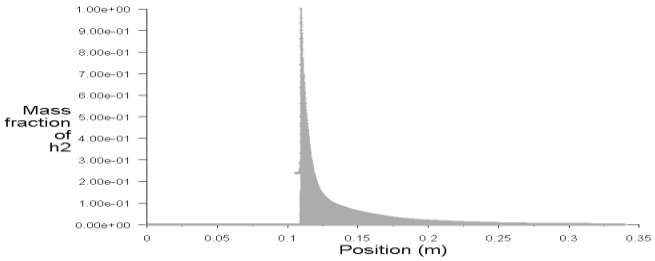


*Fig.30: Mass fraction of H2*

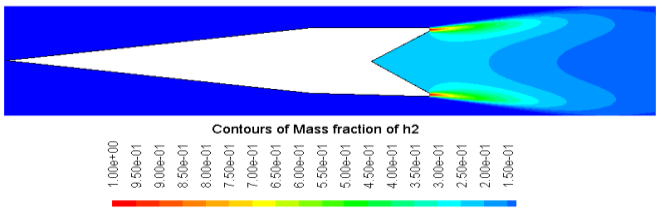


***Fig.30 contour of Mass fraction of H2***

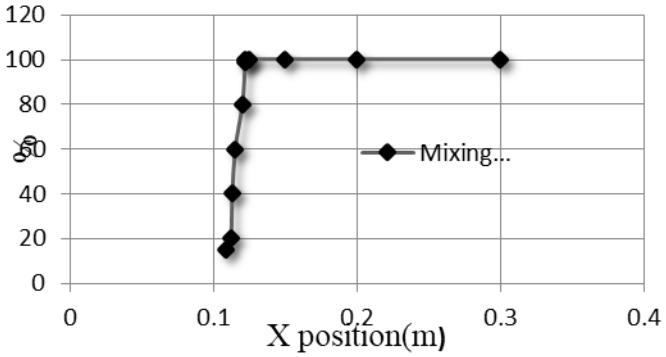


***Fig.31 Mixing efficiency***

## 15. COMBUSTION EFFICIENCY

The plots of combustion efficiency in Fig. 32 show that it reaches 100% asymptotically. It appears from this figure that combustion is complete at x ≈ 0·175m. Contours of the mass fraction of H2O are given in Fig.32. It can be seen that the maximum value for the mass fraction of H2O is reached at a distance of 0·175m, which is just downstream of the wedge. However, the distribution of the mass fraction of H2O continues to change till 0·30m, beyond which it remains the same.

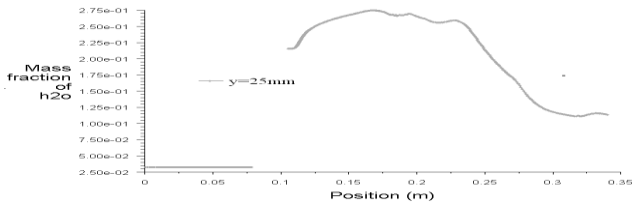


***Fig.32 Mass Fraction of H2O***

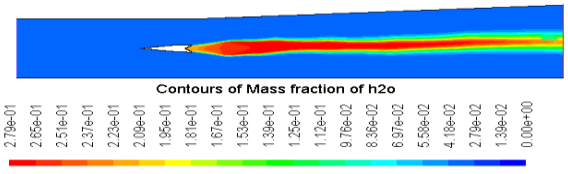


***Fig.33 Contours of mass fraction of H2O***

## 16. CONCLUSION AND SCOPE OF FUTURE WORK

### 16.1 Conclusion

In this thesis, in order to investigate the flame holding mechanism of different type of strut injectors in supersonic flow, the two-dimensional coupled implicit RANS equations, the standard k-ε turbulence model, the finite-rate/eddy-dissipation reaction model and single step chemistry are introduced to simulate the flow field of the hydrogen fueled scramjet combustor with a strut flame holder under different conditions, namely the non-reacting flow and the reacting flow. We observe the following The computational results agree reasonably well qualitatively and quantitatively with experiments, especially for static pressure distribution on the bottom wall, middle section of the combustor and axial velocity variations at different x = constant locations. In all the three injection method, static pressure of the reacting flow condition is much higher than that of the non-reacting flow condition due to the intense combustion process. There are three obvious pressure rises on the top and bottom walls of the scramjet combustor in all the injection method because of the impingement of the reflected shock wave or the expansion wave on the walls. Among all three injectors, the alternating wedge injector created a more uniform mixing region, because of this length of the combustion chamber to achieve a perfect mixing is strongly reduced. But the overall combustion performance is similar to that of a strut with circular injector and causes a larger total pressure loss. From analysis it is found that strut with planer injector giving good combustion efficiency and total pressure loss is less as compared to strut with circular injector and strut with alternating wedge injector. Combustion chamber length to be more for strut with circular injector but for planer injector it is not needed because the combustion is completed before the end of the chamber. In all the cases subsonic regions at the channel symmetry axis are responsible for flame holding. If the combustor geometry is chosen in a favorable way these subsonic zones may be kept small.

### 16.2 Scope of Future Work

Following aspects may be considered for future work: Continuation of this work could be to investigate other scramjet configurations with different types of flame holders, such as ramps or steps that are associated with smaller aerodynamic losses than the wedge configuration studied here. In this thesis two dimensional model of the Scramjet combustor is used. The logical extension to this would be to use a three dimensional model. Finally, performing a Large Eddy Simulation (LES) might yield a more accurate prediction of the large-scale turbulent structures.

## 17. ACKNOWLEDGMENT

The authors wish to thank the Principal, HOD/ Mechanical, Amrita College of Engineering and Technology Nagercoil, for the support and those who were directly or indirectly involved in this study.

## REFERENCES


1. Goyne.C.P, Rodriguez.C.G, Krauss.R.H, Mcdaniel.J.C and Mcclinton.C, Experimental and numerical study of dual mode scramjet combustor, 2002, AIAA paper 2002-5216.
2. Kim.J.H, Yoon.Y, Jeung.I.S, Huh.H and Choi.J.Y, Numerical study of mixing enhancement by shock waves in a model scramjet engine, 2003, AIAA J, 41, pp 6-13.
3. Kim.K.M, Baek.S.W and Han.C.Y, Numerical study on supersonic combustion with cavity based fuel injection, Int J Heat and Mass transfer, 2004, 47, pp 271-286.
4. Rodriguez.C.G, White.J.A and Riggins.D.W, Three-dimensional effects in modelling of dual mode scramjets, 2000, AIAA paper 2000-3704.
5. Rodriguez.C.G and Cutler.A.D, Numerical analysis of the scholar supersonic combustor, NASA-CR-2003-212689, 2003.
6. Baurle.R.A, Modelling of high speed reacting flows: Established Practices and Future Challenges, 2004, AIAA paper 2004-0267.
7. Rajasekaran.A and Babu.V, Numerical simulation of three dimensional reacting flow in a model supersonic combustor, J Propulsion and Power, 2006, 22, 4, PP 820-827.
8. M.P.Lee, B.K.McMillin, L.Palmer and R.K.Hanson, Two-dimensional imaging of combustion phenomena in a shock tube using planar laser-induced fluorescence, 1991, AIAA Paper 91-0460.
9. P. E. Dimotakis, Turbulent free shear layer mixing and combustion, High Speed Flight Propulsion Systems, 199,137, pp.45-54.
10. Dessornes and C. Jourdren, Mixing enhancement techniques in a scramjet, 1998, AIAA Paper 1998-1517.
11. T. Sunami, M. N. Wendt, and M. Nishioka, Supersonic mixing and combustion control using streamwise vortices, 1997, AIAA Paper 1998-3271, National Aerospace Laboratory.
12. L. A. Povinelli, Aerodynamic drag and fuel spreading measurements in a simulated scramjet combustion module, 1974, NASA Technical Note TN D-7674.